Dynamic and charge doping effects on the phonon dispersion of graphene

Valentin N. Popov
Faculty of Physics, University of Sofia, BG-1164 Sofia, Bulgaria

Philippe Lambin
Research Center in Physics of Matter and Radiation, Facultés Universitaires Notre Dame de la Paix, B-5000 Namur, Belgium

(Received 25 January 2010; revised manuscript received 4 May 2010; published 8 July 2010)

The phonon dispersion of graphene is calculated using a perturbative approach within a density-functional-based nonorthogonal tight-binding model. In the adiabatic approximation, the LO and the TO phonon branches are found to have a finite slope at the Γ and K points of the Brillouin zone, respectively. This linear behavior is due to strong electron-phonon coupling for electron wave vector close to the K point and is a signature of the Kohn anomaly. The explicit account of the dynamic effects results in a strong modification of these phonon branches as well as in a significant broadening of their linewidth in the vicinity of the Γ and K points. In particular, the finite slope of the phonon branches turns to zero. The charge doping of graphene changes the LO and TO branches in the vicinity of the two points and essentially removes the Kohn anomaly with the increase in the doping level. The obtained results are in a good agreement with available experimental data.

DOI: 10.1103/PhysRevB.82.045406 PACS number(s): 63.22.Rc, 78.30.Na, 78.67.Wj, 73.22.Pr

I. INTRODUCTION

For a long-time monolayer graphite sheets (graphene) have been thought to be unstable under ambient conditions. Recently, high-quality monolayer graphene flakes have been produced by mechanical exfoliation[1] and by epitaxial growth.[2] Graphene is a zero-gap semiconductor with a linear dispersion of the electronic bands close to the Fermi energy at the K and K′ points of the Brillouin zone and can easily be turned into either electron or hole conductor by charge doping.[3,4] In addition, electron scattering is very small up to room temperatures in favor of ballistic electronic transport.[5] These features of graphene make it a perspective candidate for electronic devices, which are scalable to nanometer sizes.

The level of doping of graphene can be monitored by Raman spectroscopy. The Raman spectrum of graphene is dominated by the G line, arising from one-phonon inelastic scattering of light from the G mode, which is the only Raman-active phonon. It is a doubly degenerate phonon with symmetry E_{2g}, frequency of ≈ 1582 cm^{-1}, and in-plane LO and TO polarized components. Recent measurements of the frequency shift and the linewidth of the G line of graphene vs doping level have revealed strong dependence of these quantities on the Fermi energy shift E_F, which can be explained with dynamic effects associated with strong electron-phonon coupling.[3,4,6] These results have been supported by calculations using time-dependent perturbation theory within the density-functional theory (DFT).[7]

Strong electron-phonon coupling has been predicted for the TO-branch phonon at the K point with symmetry A_1' (Refs. 8 and 9) and an in-plane breathinglike motion of the hexagons;[10] further on, it will be referred to as the A_1' mode. This suggests a significant modification of the TO branch around K point, which should be considered in the modeling of defect-induced and two-phonon resonance Raman scattering. As far as we are aware, no theoretical results on this specific problem have been reported so far.

Here, we study the dynamic and charge doping effects on the phonon dispersion of graphene by use of a perturbative approach[11] within a density-functional-based nonorthogonal tight-binding (NTB) model.[12] We recover the DFT data for the frequency shift and linewidth of the G mode and append them with results for the A_1' mode and for the LO and TO branches in the vicinity of the Γ and K points. The paper is organized as follows. The general theoretical background is given in Sec. II while the details of the calculation of the electronic structure, phonon dispersion, and Raman intensity are provided in Appendices A and C, respectively. The calculated phonon dispersion and linewidth are presented and discussed in the case of the adiabatic approximation (Sec. III A), dynamic corrections (Sec. III B), and charge doping (Sec. III C). The paper ends up with conclusions (Sec. IV).

II. THEORETICAL BACKGROUND

We calculate the electronic band structure of graphene within the NTB model with four valence electrons per carbon atom[12] (see Appendix A). This model makes use of the matrix elements of the Hamiltonian and overlap matrix elements derived from first principles[13] and therefore does not rely on any adjustable parameters. It also allows one to estimate the total energy and forces on atoms. This feature is utilized for relaxation of the atomic structure of graphene.

A perturbative approach within the NTB model is used to calculate the phonon dispersion of graphene in the adiabatic approximation[11] (see Appendix B). The dynamical matrix is derived by expanding the energy of the crystal lattice of graphene, distorted by a phonon, in a power series of the atomic displacements up to second order. The obtained expansion contains terms with second-order variations in the matrix elements in the atomic displacements treated in first-order perturbation theory and terms with first-order variations in the matrix elements in the atomic displacements treated in second-order perturbation theory. The perturbative approach has the advantage over the frozen-phonon one of avoiding the computationally expensive enlarging of the original cell in the calculations of forces on atoms. More-

over, in the former, the dynamical matrix is derived in a single step.

The fact that graphene is a zero-gap semiconductor has crucial consequences on the phonon dispersion. The presence of electronic states close to the Fermi energy around the two points K and K′ of the Brillouin zone favors scattering of electrons by phonons between such states. The scattering is more effective for phonons with stronger electron-phonon coupling. This is indeed the case with the LO and TO phonons close to the Γ and K points, resulting in finite slopes of these branches, which is a signature of the Kohn anomaly in graphene.[8,11]

Another consequence of the strong electron-phonon coupling is the renormalization of the phonon frequency and linewidth and the significant modification of the Kohn anomaly associated with it. The renormalization is described here by going beyond the adiabatic approximation and explicitly accounting for the dynamic effects.[7]

Finally, we adopt the quantum-mechanical description of the Raman-scattering process in which the system of the electrons and phonons of the system, and photons of the electromagnetic radiation, and their interactions are considered[14] (see Appendix C). This description allows for the account of the finite electron and phonon lifetime due to scattering processes.[15]

III. RESULTS AND DISCUSSION

A. Adiabatic approximation

The atomic structure of graphene was relaxed within the NTB model by use of a 600×600 Monkhorst-Pack mesh in the Brillouin zone until the residual forces on all atoms decreased below 0.01 eV/Å. The phonon calculations were performed for the relaxed structure by use of the dynamical matrix, Eq. (B5). The large number of **k** points ensures accuracy of the phonon frequencies within 1 cm^{-1}. The NTB model is known to overestimate the optical branches of graphene by about 11% (Ref. 11) but the scaling of the phonon frequencies by a factor of 0.9 yields a very good agreement with the available experimental data, especially, in the high-frequency region.[10,16,17] For this reason and for comparison with experimental and other theoretical data, all obtained phonon frequencies are scaled by this factor.

The calculated phonon dispersion of graphene along the high-symmetry directions ΓK, KM, and ΓM is shown in Fig. 1. It has been impossible to determine experimentally the frequency of the TO branch close to the K point and, in particular, the A_1'-mode frequency because of the dramatic decrease in the phonon lifetime.[10] The inelastic x-ray scattering data[10,17] and Raman data[18] indicate that this mode should be close to the LO and LA branches crossing at the K point. The DFT calculations position it at least ≈100 cm^{-1} above this crossing.[8,17] The accurate treatment of the electron correlations within the Green's function approach using the GW method has predicted this mode to be by 14 cm^{-1} below the crossing.[19] The NTB model yields the crossing of LO and LA branches at 1267 cm^{-1} and the A_1'-mode frequency to be by 32 cm^{-1} below the crossing,[11] in fair agreement with the GW results. The NTB model has the advantage over the *ab initio* models of inexpensive calculation of the phonon frequencies and eigenvectors at any point of the Brillouin zone and the consequent easy estimation of the changes in the phonon dispersion of graphene due to dynamic and doping effects. Because of the importance of the behavior of the LO and TO branches around the Γ and K points, we present and discuss only results for these two branches along the ΓKM direction.

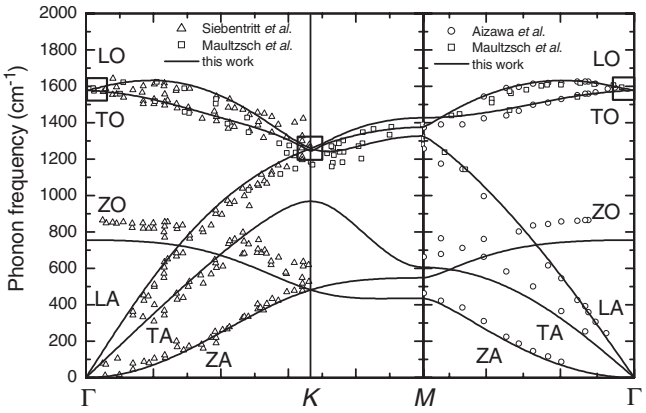

FIG. 1. Calculated phonon dispersion of graphene along high-symmetry directions in the Brillouin zone in comparison with available experimental data. The phonon branches are marked with acronyms of two letters with the following meaning: "L"—longitudinal, "T"—transverse, "Z"—out of plane, "O"—optical, and "A"—acoustic. The regions with most significant changes in the branches due to dynamic effects are enclosed in rectangles.

The calculated phonon dispersion shows linear wave-vector dependence of the LO and TO branches at the Γ and K points, respectively, as a signature of the Kohn anomaly[8] (Fig. 1). The temperature dependence of the phonon dispersion was studied here by smearing of the electron distribution close to the Fermi energy by means of the Fermi-Dirac distribution function. The results for several temperatures show that the effect of temperature on the linearity of the mentioned branches is negligible up to room temperature, though the frequencies of the G mode and A_1' mode exhibit small decrease and increase, respectively. For these reasons, here we report results only for $T=300$ K.

The convergence of the dynamical matrix could be achieved by use of a large number of **k** points, which can be explained with the zero gap of graphene at the K and K′ points of the Brillouin zone.[11] Mathematically, this is due to terms of the dynamical matrix with energy denominator, vanishing at the two points. These terms can be written in the general form [see Eq. (B2)]

$$\sum_{\mathbf{k}vc}\frac{M_{\mathbf{k}v,\mathbf{k}+\mathbf{q}c}}{E_{\mathbf{k}v}-E_{\mathbf{k}+\mathbf{q}c}}. \tag{1}$$

Here, $E_{\mathbf{k}v}$ and $E_{\mathbf{k}+\mathbf{q}c}$ are the energies of the valence and conduction bands, respectively, depending on the electron wave vector **k** and the phonon wave vector **q**. The quantity $M_{\mathbf{k}v,\mathbf{k}+\mathbf{q}c}$ consists of first-order variations in the band-structure matrix elements in the atomic displacements. The summation is over the Brillouin zone and over the valence

and conduction bands. The denominator of Eq. (1) vanishes for scattering of an electron by a zone-center phonon at the K or K′ point or scattering of an electron by a K point phonon between the K and K′ points. The sum Eq. (1) is actually convergent, which is readily seen if one considers linear electronic bands close to these two points and assumes a constant numerator. The sum can be transformed into an integral over $k \equiv |\mathbf{k}|$ between zero and some cutoff value with an area element $2\pi k dk$. The direct integration then yields a finite value.

The slopes of the LO and TO branches at the Γ and K points, β_Γ and β_K, respectively, can be directly associated with the electron-phonon coupling constants.[8] The previous DFT values[8] $\beta_\Gamma = 340$ cm^{-1} and $\beta_K = 973$ cm^{-1} have been corrected by recent GW data $\beta_\Gamma = 487$ cm^{-1} (Ref. 20) and $\beta_K = 1504$ cm^{-1} (Ref. 19). The NTB model yields $\beta_\Gamma = 475$ cm^{-1} and $\beta_K = 1242$ cm^{-1}, in good agreement with the GW data, which justifies the use of the NTB model for simulation of processes and phenomena with important electron-phonon coupling.

B. Dynamic effects

The strong electron-phonon interactions give rise to modifications of the phonon dispersion around the Γ and K points. These dynamic corrections to the phonon frequency, $\Delta\omega$, and the phonon linewidth, $\Delta\Gamma$, can be derived from the dynamical matrix, obtained in the adiabatic approximation, by adding $\hbar\omega + i\delta$ to the energy denominator in Eq. (1), where ω is the phonon frequency in the adiabatic approximation and δ is a small positive number.[8,21,22] Considering the corrections $\Delta\omega$ and $\Delta\Gamma$ to be small compared to ω, one can derive the following expressions:

$$\Delta\omega = \frac{1}{2\omega}\mathrm{Re}\{\mathbf{e}^+[D(\hbar\omega + i\delta) - D(0)]\mathbf{e}\}, \tag{2}$$

$$\Delta\Gamma = \frac{\pi}{2\omega}\mathrm{Im}[\mathbf{e}^+ D(\hbar\omega + i\delta)\mathbf{e}]. \tag{3}$$

Here, $D(\hbar\omega + i\delta)$ is the corrected dynamical matrix, $D(0)$ is the dynamical matrix, derived in the adiabatic approximation, and $\mathbf{e}$ is the phonon eigenvector.

The dynamic corrections were calculated by means of Eqs. (2) and (3). The obtained high-frequency phonon dispersion in the vicinity of the Γ and K points is shown in Figs. 2 and 3. It is clear that while the G-mode and A_1'-mode frequencies have zero dynamic corrections, major changes in the phonon dispersion are present for nonzero phonon wave vectors. The most important one is the appearance of a zero slope of the LO and TO branches at the two points in place of the finite one. In the vicinity of the Γ point, the LO and TO branches remain almost flat up to some phonon wave vector q_Γ (Fig. 2), where the LO branch has a kink and the TO branch reaches a minimum. Similarly, the TO branch at the K point has an almost flat region of size of $\sim 2q_K$, determined by some wave vector q_K relative to the K point (Fig. 3). These features of the corrected phonon dispersion can be considered as signatures of the Kohn anomaly. For larger wave vectors both LO and TO branches tend to those obtained in the adiabatic approximation.

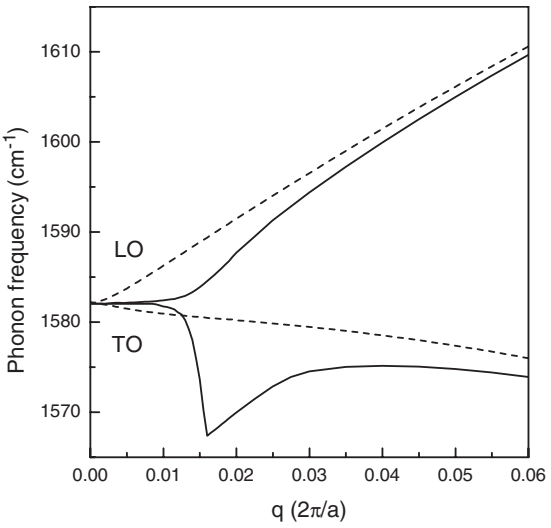

FIG. 2. Calculated LO and TO branches close to the Γ point in the adiabatic approximation (dashed lines) and with dynamic effects (solid lines).

The correction to the linewidth of the LO and TO phonons around the Γ and K points is shown in Figs. 4 and 5. As seen in Fig. 4, with the increase in the wave vector from the Γ point, the linewidth for the TO branch reaches a maximum at wave vector q_Γ and then decreases to zero while the linewidth for the LO branch decreases monotonously to zero. The linewidth for the TO branch reaches a maximum at the K point and decreases rapidly away from it (Fig. 5).

The behavior of $\Delta\omega$ and $\Delta\Gamma$ can be explained by arguments, similar to those, provided for metallic nanotubes.[23] In the latter study, the integration over the one-dimensional

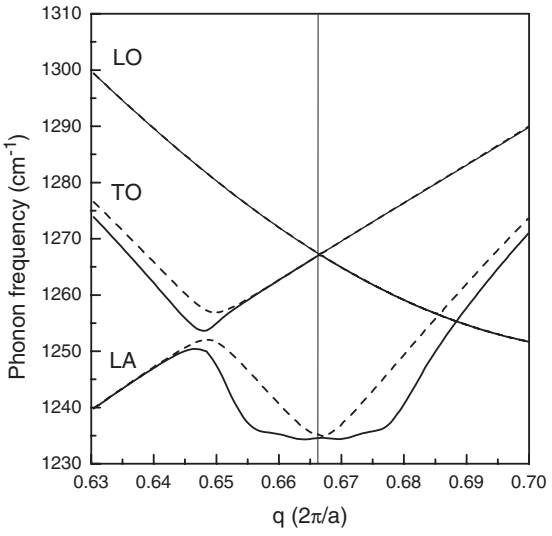

FIG. 3. Calculated LO, TO, and LA branches close to the K point along the ΓKM direction in the adiabatic approximation (dashed lines) and with dynamic effects (solid lines). The position of the K point is marked with a vertical line. Note the avoided crossing of the TO and LA branches at ≈0.65 splitting the TO branch into two parts.

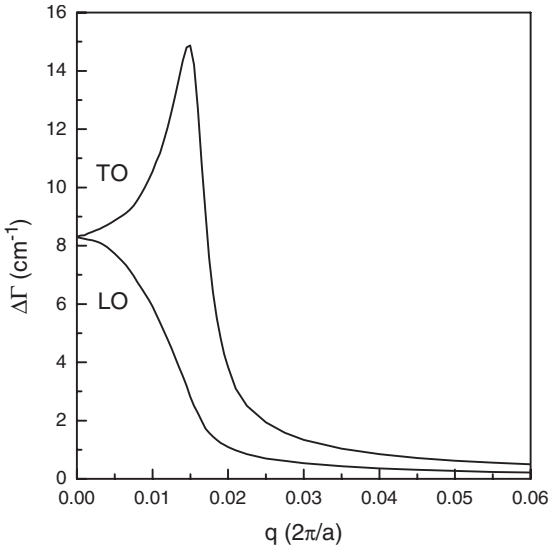

FIG. 4. Calculated phonon linewidth $\Delta\Gamma$ for the LO and TO branches close to the Γ point.

wave vector [see Eq. (1) with $\hbar\omega$ added to the denominator] is split into three regions: $(-\infty,-q_{\Gamma,K})$, $[-q_{\Gamma,K},0]$, and $(0,\infty)$, where $q_{\Gamma,K}\sim\hbar\omega_{\Gamma,K}/\beta_F$, β_F is the slope of the electronic bands at the Fermi energy and the indices Γ and K denote phonons in the vicinity of these two points. The wave vectors $q_{\Gamma,K}$ and 0 separate regions with backscattering and forward scattering of electrons. The different dependence of $\Delta\omega$ and $\Delta\Gamma$ on the wave vector for the LO and TO branches stems in the fact that the electron-phonon coupling in metallic nanotubes is nonzero only for backscattering and forward scattering of electrons from LO and TO phonons close to the Γ point, respectively, and for backscattering from TO phonons close to the K point. It has been proven analytically that this character of the electron scattering gives rise to a dip in the

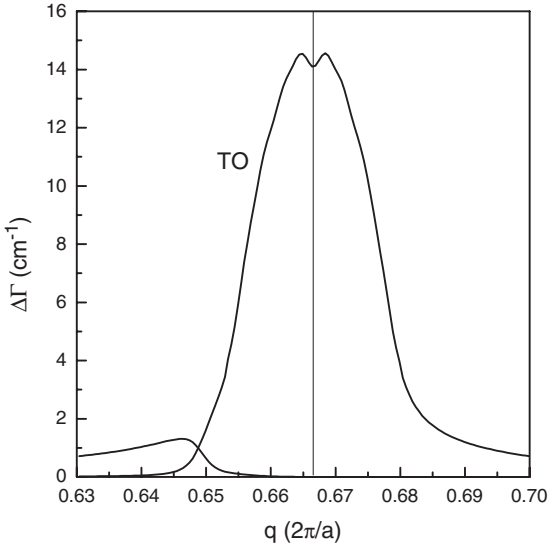

FIG. 5. Calculated phonon linewidth $\Delta\Gamma$ for the TO branch close to the K point along the ΓKM direction. The position of the K point is marked with a vertical line. The two curves correspond to the two parts of the TO branch in Fig. 3.

LO branch and a singularity in the TO branch at phonon wave vector q_Γ. From the same study, though not explicitly written, it follows also that the linewidth of the LO branch has a maximum at the Γ point and decreases away from it, and the linewidth of the TO branch has a maximum at q_Γ and decreases rapidly away from it. In graphene, due to the two dimensionality of the structure, such analytical derivations are difficult to accomplish. However, qualitative conclusions can be drawn taking into account that the electron scattering from LO and TO phonons close to the Γ point is predominantly backscattering and forward scattering, respectively, and the scattering from TO phonons close to the K point is predominantly backscattering [see Eq. (6) in Ref. 8]. This result implies the existence of characteristic phonon wave vectors with length $q_{\Gamma,K}$ for graphene as well and similar behavior of the phonon dispersion and linewidth in both metallic nanotubes and graphene, as summarized in the previous two paragraphs.

In the NTB model, $\beta_F=12.8$ eV for wave vector in units of $2\pi/a$, where a is the lattice parameter of graphene. This value of the slope corresponds to electron velocity at the Fermi energy $v_F=8.0\times10^5$ m/s. For the G mode $\omega_\Gamma=0.196$ eV and $q_\Gamma=0.0153$, and for the A_1' mode $\omega_K=0.154$ eV and $q_K=0.0120$. Therefore, the regions of importance of the dynamic effects are circles centered at the Γ and K points of size $\approx$50 times smaller than the size of the Brillouin zone of graphene. Outside these regions, the dynamic effects are negligible and the adiabatic approximation yields reasonable predictions for the phonon dispersion.

C. Doping effects

The charge doping generally modifies the electronic structure of graphene. In the band approximation, the introduction of charges to the conduction bands or the removal of charges from the valence bands simply changes the band contribution of the total energy and the system relaxes to a state with a different lattice parameter. For doping levels of $\sim10^{12}$ cm^{-2}, corresponding to Fermi energy shifts $E_F\sim0.1$ eV, the variation in the lattice parameter is negligible (see also Ref. 7). For these reasons, the calculations for doped graphene were performed for the relaxed structure at zero doping.

The general effect of the charge doping of graphene is an upshift of the phonon dispersion, the most affected being the LO and TO phonon branches close to the Γ and K points (Figs. 6 and 7). The characteristic features, due to the dynamic correction, e.g., the flat regions around these points, the kink of the LO branch, and the pronounced dip of the TO branch at q_Γ, tend to be gradually smeared out with the increase in the doping level. For $|E_F|=0.3$ eV the flat region is still present but the dip is no longer noticeable. For the same doping, the frequencies of the G mode and the A_1' mode become higher by 11 cm^{-1} and 32 cm^{-1}, respectively, compared to undoped graphene. With the increase in the phonon wave vector, these corrections become smaller and outside the regions of size q_Γ and q_K they are negligible. The doping effect on the phonon linewidth is illustrated in Figs. 8 and 9. The increase in the doping level results in a decrease in the correction to the phonon linewidth. For $|E_F|=0.3$ eV this correction is already below 1 cm^{-1}.

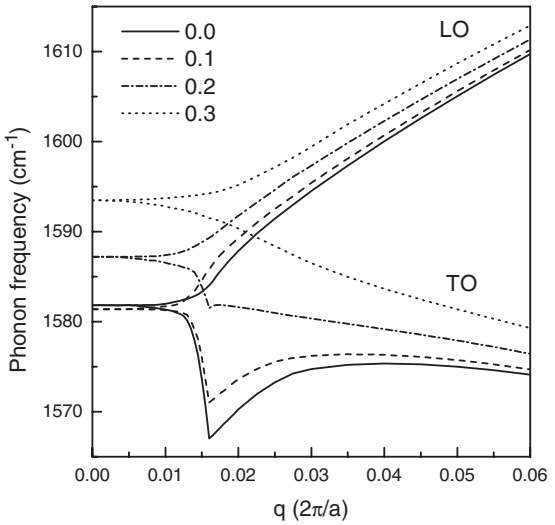

FIG. 6. Calculated LO and TO branches with included dynamic effects close to the Γ point for four different Fermi energy shifts E_F=0.0, 0.1, 0.2, and 0.3 eV.

Figures 10 and 11 show that the frequencies of the G mode and A_1' mode are almost constant for Fermi energy shift $|E_F|$ up to 0.1 eV and 0.08 eV, respectively, and increase quasilinearly outside these regions. The calculated G-mode and A_1'-mode linewidths (Figs. 12 and 13) are significant for $|E_F|$ up to ≈0.1 eV but become small outside this region, decreasing steeply with the increase in the Fermi energy shift. The zero-doping linewidth has a maximum value of 8.3 cm^{-1} for the G mode and 14.2 cm^{-1} for the A_1' mode. The former value agrees well with available experimental ones of 8 cm^{-1} (Ref. 3) and 8.5 cm^{-1} (Ref. 4).

The dependence of the frequency and linewidth of the G mode on the doping level can be explained with the effective phonon renormalization via electron-hole creation and annihilation. As it is seen from Eq. (1) with $\hbar\omega$ added to the

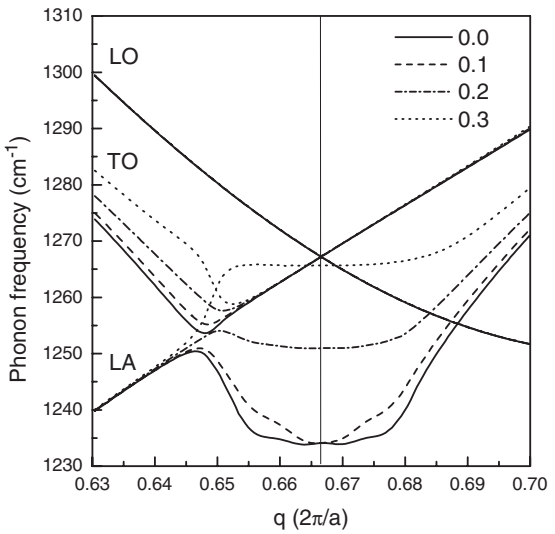

FIG. 7. Calculated LO, TO, and LA branches with included dynamic effects close to the K point along the ΓKM direction for four different Fermi energy shifts E_F=0.0, 0.1, 0.2, and 0.3 eV. The position of the K point is marked with a vertical line.

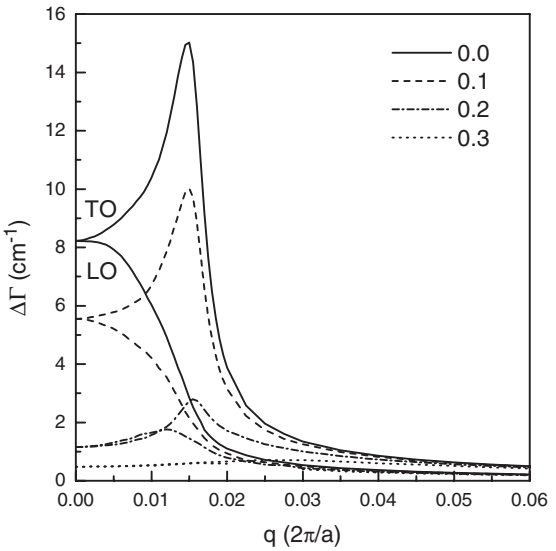

FIG. 8. Calculated phonon linewidth ΔΓ for the LO and TO branches close to the Γ point for four different Fermi energy shifts E_F=0.0, 0.1, 0.2, and 0.3 eV.

denominator to account for dynamic effects, such processes can take place if occupied (empty) and empty (occupied) states are present in the valence and conduction bands, respectively, which satisfy the condition $E_{\mathbf{k}c}-E_{\mathbf{k}v}=\hbar\omega$. Such states exists for doping levels up to $|E_F|=\hbar\omega/2$. Therefore, this value of E_F determines the crossover between the regime with strong and weak phonon renormalization. The behavior of $\Delta(\hbar\omega)$ and ΔΓ of the G mode vs E_F at T=0 K can be described approximately by the formulas[3,4]

$$\Delta(\hbar\omega) = \alpha\left\{|E_F| + \frac{\hbar\omega}{4}\ln\left|\frac{2|E_F|-\hbar\omega}{2|E_F|+\hbar\omega}\right|\right\}, \qquad (4)$$

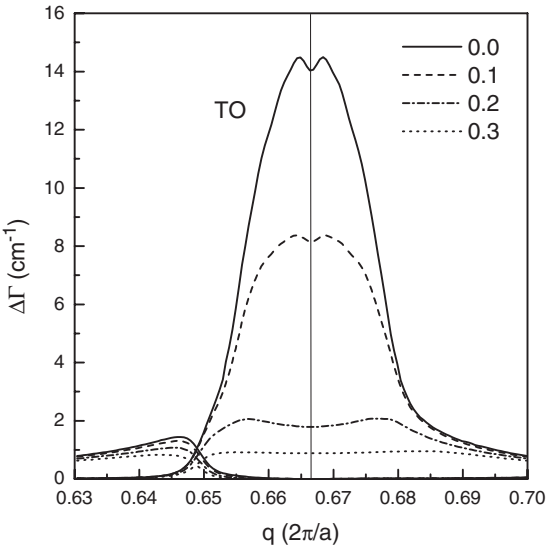

FIG. 9. Calculated phonon linewidth ΔΓ for the TO branch close to the K point along the ΓKM direction for four different Fermi energy shifts E_F=0.0, 0.1, 0.2, and 0.3 eV. The position of the K point is marked with a vertical line.

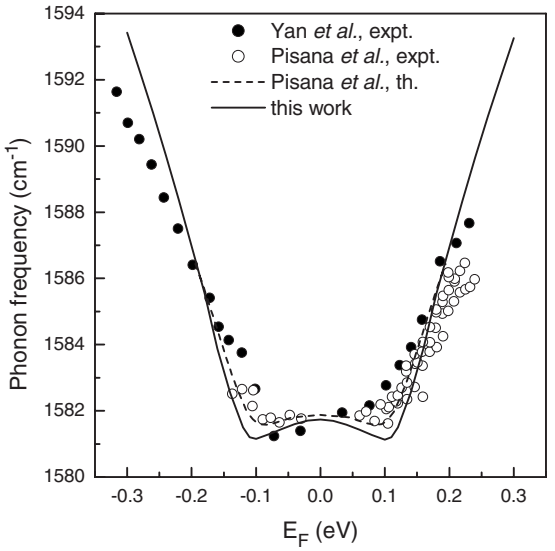

FIG. 10. Calculated G-mode frequency vs Fermi energy shift E_F in comparison with experimental data and theoretical predictions.

$$\Delta\Gamma = \begin{cases} \alpha\dfrac{\pi\hbar\omega}{4} & |E_F| \le \dfrac{\hbar\omega}{2} \\ 0 & |E_F| > \dfrac{\hbar\omega}{2}. \end{cases} \tag{5}$$

Here $\alpha = AD^2/2\pi\hbar\omega M v_F^2$, A is the unit-cell area, D is the electron-phonon coupling constant, and M is the carbon atom mass. According to Eq. (4), $\Delta(\hbar\omega)$ has two logarithmic singularities at $|E_F| = \hbar\omega/2$ and linear asymptotic behavior for large $|E_F|$. Equation (5) yields a finite linewidth correction for $|E_F| \le \hbar\omega/2$ and zero, otherwise. For finite temperatures, the logarithmic singularities are smeared out and the rectangular shape of the linewidth is smoothened, as can be observed from the obtained results in Figs. 10 and 12. Expressions, analogous to Eqs. (4) and (5), can be derived for the frequency and linewidth of the A_1' mode.

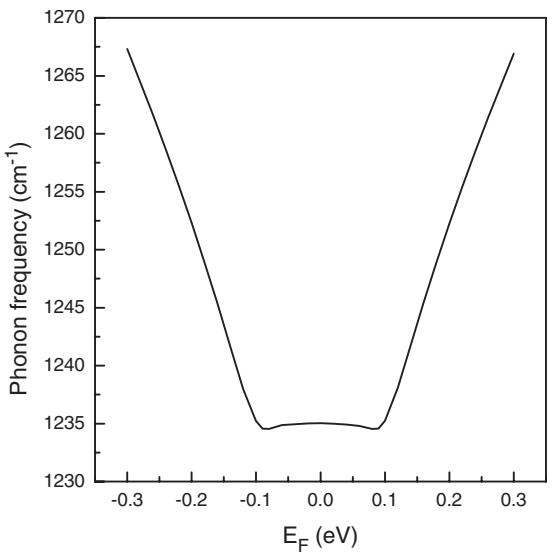

FIG. 11. Calculated A_1'-mode frequency vs Fermi energy shift E_F.

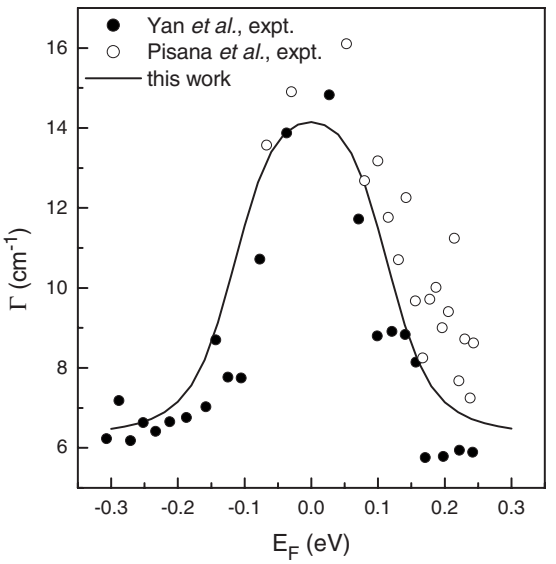

FIG. 12. Calculated phonon linewidth of the G-mode $\Gamma_0 + \Delta\Gamma$ vs Fermi energy shift E_F in comparison with available experimental data. $\Gamma_0 = 6$ cm^{-1} is the contribution to the linewidth, which is not associated with electron-phonon coupling.

From the slope of the calculated frequency shift of G mode vs doping one can determine the electron-phonon coupling constant by use of the asymptotic formula:[4] $\Delta(\hbar\omega) = \alpha|E_F|$. From our results we obtain $\alpha = 52$ cm^{-1}/eV and $D = 11.4$ eV/Å. This value corresponds to the experimental values of 12.6–14.1 eV/Å (Ref. 4) and to the theoretical one of 13.5 eV/Å, derived within the DFT.[7] A more precise determination of the electron-phonon coupling D can be done from the maximum of the phonon linewidth via the formula:[4] $\Delta\Gamma = AD^2/8Mv_F^2$. Thus, we obtain $D = 11.2$ eV/Å for the coupling at the Γ point. Previous NTB calculations of

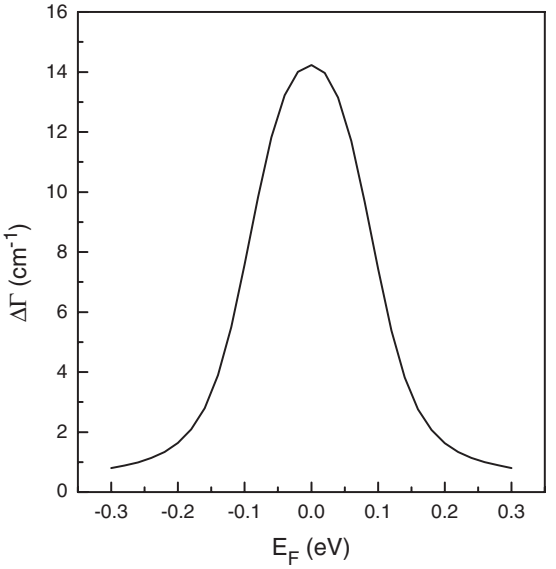

FIG. 13. Calculated phonon linewidth of the A_1' mode vs Fermi energy shift E_F.

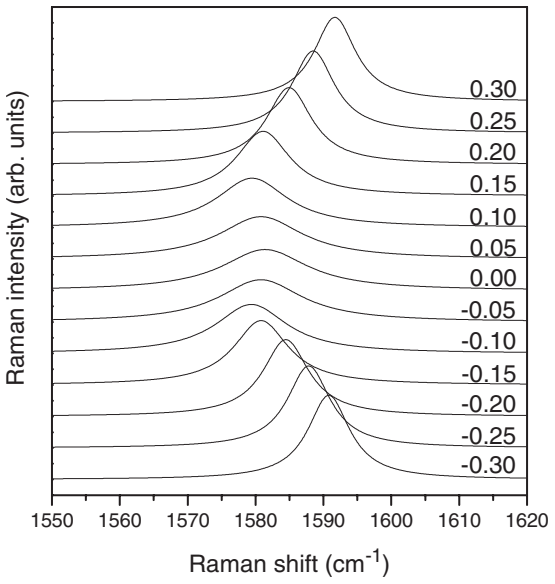

FIG. 14. Calculated Raman spectra in the high-frequency region including the G mode for different Fermi energy shifts E_F from −0.3 to 0.3 eV.

the electron-phonon coupling matrix elements of nanotubes yielded in the large-radius limit $D=12.8$ eV/Å. Bearing in mind that D determines the squared phonon frequencies, the scaling of the frequencies by 0.9 corresponds to scaling of D by $0.9^2=0.81$. Therefore, the scaled value of the latter matrix element should be ≈ 10.4 eV/Å, which is close to that, derived from the linewidth here. Similarly, for the electron-phonon coupling at the K point (Fig. 13) we get $D=14.7$ eV/Å, which is smaller than the previous NTB value[9] of 18.1 eV/Å. However, both values are in a good agreement with each other if the NTB value is downscaled by a factor of 0.81.

D. Raman intensity

Finally, we calculate the resonance Raman intensity of the G mode with dynamic corrections as a function of the doping level for parallel scattering geometry (see Appendix C). The intensity was averaged over all possible orientations in space of the laser photon polarization for better correspondence with the common experimental setup. The effect of the finite phonon linewidth is accounted for by a Lorentzian broadening of the Raman line.[15] The calculated Raman spectra of graphene, shown in Fig. 14, exhibit an increasing blueshift of the G-line position with the increase in the doping level while the G-line peak value increases abruptly from an almost constant value to a larger one at $|E_F|\approx 0.1$ eV. This behavior is observed in the experimental Raman spectra.[4]

IV. CONCLUSIONS

We showed that the dynamic corrections have significant effect on the phonon dispersion of graphene in the vicinity of the Γ and K points and modify the Kohn anomaly, predicted in the adiabatic approximation. We reproduce the *ab initio* results for the G-mode frequency and predict the dynamic correction of the phonon dispersion, which is important for interpretation of the experimental data on double-resonance Raman scattering as well as for modeling of electron-phonon scattering processes in graphene. We also studied the doping dependence of the phonon dispersion close to the two special points, the major doping effect being the smearing out of the Kohn anomaly with the increase in the doping level.

ACKNOWLEDGMENTS

V.N.P. was supported partly by Marie-Curie European Reintegration under Grant No. MERG-CT-2007-201227 within the Seventh European Community Framework Programme and partly by NSF under Grant No. DO 02-136/15.12.2008 (IRC-CoSiM).

APPENDIX A

Graphene has a two-dimensional periodic structure with two carbon atoms in the unit cell. Within the NTB model with four valence electrons per carbon atom,[12,13] the electronic problem is reduced to the following matrix eigenvalue equation:

$$\sum_{r'} (H_{\mathbf{k}rr'} - E_{\mathbf{k}} S_{\mathbf{k}rr'}) c_{\mathbf{k}r'} = 0. \tag{A1}$$

Here $\mathbf{k}$ is the two-dimensional wave vector and the index r labels the valence orbitals of the unit cell, $r=1,2,\ldots,8$. The quantities $H_{\mathbf{k}rr'}$ and $S_{\mathbf{k}rr'}$ are given by the expressions

$$H_{\mathbf{k}rr'} = \sum_{\mathbf{l}} e^{i\mathbf{k}\cdot\mathbf{R}(\mathbf{l})} H_{rr'}(R) \tag{A2}$$

and

$$S_{\mathbf{k}rr'} = \sum_{\mathbf{l}} e^{i\mathbf{k}\cdot\mathbf{R}(\mathbf{l})} S_{rr'}(R), \tag{A3}$$

where $H_{rr'}(R)$ and $S_{rr'}(R)$ are the matrix elements of the Hamiltonian and the overlap matrix elements,[13] respectively, between orbitals r and r' centered at two atoms at a distance R. The quantity $E_{\mathbf{k}}$ is the one-electron eigenenergy and $c_{\mathbf{k}r}$ are the coefficients in the expansion of the one-electron wave function as a linear combination of the atomic orbitals of the unit cell. The solutions to the eigenvalue equation, Eq. (A1), are $E_{\mathbf{k}m}$ and $c_{\mathbf{k}mr}$, $m=1,2,\ldots,8$.

The total energy of the system and the forces acting on the atoms are necessary for relaxing the atomic structure of graphene. The total energy is given by the expression

$$E = \sum_{\mathbf{k}m}^{occ} E_{\mathbf{k}m} + \frac{1}{2} \sum_{ij(i\neq j)} \phi(R_{ij}), \tag{A4}$$

where the first term is the band energy E_{BS} (the summation is over all occupied states) and the second term is the repulsive energy E_{rep}, expressed as the sum of repulsive pair potentials[13] $\phi(R)$ between pairs of atoms at a distance R. The band contribution to the forces on the atoms is given by the Hellmann-Feynman theorem. The repulsive contribution to the force is equal to the first derivative of the total repulsive energy with respect to the atomic position vector.

APPENDIX B

In the perturbative approach within the NTB model,[11] one determines the response of the electrons to the atomic displacements in the linear-response approximation. Namely, the dynamical matrix is obtained from the change in the total energy due to a static lattice deformation (a phonon) with a two-dimensional wave vector $\mathbf{q}$

$$\mathbf{u}(\mathbf{l}\kappa) = \mathbf{e}(\kappa|\mathbf{q})e^{i\mathbf{q}\cdot\mathbf{R}(\mathbf{l})} + \text{c.c.} \tag{B1}$$

Here, $\mathbf{e}(\kappa|\mathbf{q})$ is the phonon eigenvector and the index κ labels the atoms in the unit cell, $\kappa=1,2$.

The band contribution to the energy change, derived in second-order perturbation theory, is given by (see also Ref. 24)

$$\begin{aligned} E_{BS} - E_{BS}^{(0)} = & \sum_{\mathbf{k}m} \mathbf{c}_{\mathbf{k}m}^{+}(\mathbf{H}^{(2)} - E_{\mathbf{k}m}\mathbf{S}^{(2)})\mathbf{c}_{\mathbf{k}m} \\ & - 2\sum_{\mathbf{k}mm'} \mathbf{c}_{\mathbf{k}m}^{+}(\mathbf{H}_{0+}^{(1)} - E_{\mathbf{k}m}\mathbf{S}_{0+}^{(1)})\mathbf{c}_{\mathbf{k}+\mathbf{q}m'}\mathbf{c}_{\mathbf{k}+\mathbf{q}m'}^{+}\mathbf{S}_{0+}^{(1)}\mathbf{c}_{\mathbf{k}m} \\ & - 2\sum_{\mathbf{k}mm'} \mathbf{c}_{\mathbf{k}m}^{+}(\mathbf{H}_{0-}^{(1)} - E_{\mathbf{k}m}\mathbf{S}_{0-}^{(1)})\mathbf{c}_{\mathbf{k}-qm'}\mathbf{c}_{\mathbf{k}-qm'}^{+}\mathbf{S}_{0-}^{(1)}\mathbf{c}_{\mathbf{k}m} \\ & + 2\sum_{\mathbf{k}mm'} (E_{\mathbf{k}m} - E_{\mathbf{k}+\mathbf{q}m'})^{-1}\mathbf{c}_{\mathbf{k}m}^{+}(\mathbf{H}_{0+}^{(1)} - E_{\mathbf{k}m}\mathbf{S}_{0+}^{(1)}) \\ & \times \mathbf{c}_{\mathbf{k}+\mathbf{q}m'}\mathbf{c}_{\mathbf{k}+\mathbf{q}m'}^{+}(\mathbf{H}_{+0}^{(1)} - E_{\mathbf{k}m}\mathbf{S}_{+0}^{(1)})\mathbf{c}_{\mathbf{k}m} \\ & + 2\sum_{\mathbf{k}mm'} (E_{\mathbf{k}m} - E_{\mathbf{k}-\mathbf{q}m'})^{-1}\mathbf{c}_{\mathbf{k}m}^{+}(\mathbf{H}_{0-}^{(1)} - E_{\mathbf{k}m}\mathbf{S}_{0-}^{(1)}) \\ & \times \mathbf{c}_{\mathbf{k}-\mathbf{q}m'}\mathbf{c}_{\mathbf{k}-\mathbf{q}m'}^{+}(\mathbf{H}_{-0}^{(1)} - E_{\mathbf{k}m}\mathbf{S}_{-0}^{(1)})\mathbf{c}_{\mathbf{k}m}. \end{aligned} \tag{B2}$$

Here, in the second and third lines the indices m and m' run over all occupied states while in the fourth and fifth lines the index m (m') runs over all occupied (unoccupied) states. $\mathbf{H}^{(1)}$ and $\mathbf{H}^{(2)}$ are first- and second-order changes in the matrix $\mathbf{H}$ given by the expressions

$$\mathbf{H}^{(2)} = \frac{1}{2}\sum_{\mathbf{l}'\alpha\beta} e^{i\mathbf{k}\cdot\mathbf{R}(\mathbf{l}')}\nabla_\alpha\nabla_\beta\mathbf{H}u_\alpha(\mathbf{0}\kappa\mathbf{l}'\kappa')u_\beta(\mathbf{0}\kappa\mathbf{l}'\kappa'), \tag{B3}$$

$$\mathbf{H}^{(1)} = \sum_{\mathbf{l}'\alpha} e^{i\mathbf{k}\cdot\mathbf{R}(\mathbf{l}')}\nabla_\alpha\mathbf{H}u_\alpha(\mathbf{0}\kappa\mathbf{l}'\kappa'), \tag{B4}$$

where $\nabla_\alpha\mathbf{H}$ and $\nabla_\alpha\nabla_\beta\mathbf{H}$ are partial derivatives with respect to $u_\alpha(\mathbf{0}\kappa\mathbf{l}'\kappa') \equiv u_\alpha(\mathbf{0}\kappa) - u_\alpha(\mathbf{l}'\kappa')$ and the exponentials are removed from u_α and u_β; α and β are tensor indices, $\alpha,\beta=1,2,3$. $\mathbf{H}_{0+}^{(1)}$, $\mathbf{H}_{0-}^{(1)}$, $\mathbf{H}_{+0}^{(1)}$, and $\mathbf{H}_{-0}^{(1)}$ derive from Eq. (B4) by substitution of $\mathbf{u}(\mathbf{0}\kappa\mathbf{l}'\kappa')$ with $\mathbf{e}^*(\kappa)e^{i\mathbf{q}\cdot\mathbf{R}(\mathbf{l}')} - \mathbf{e}^*(\kappa')$, $\mathbf{e}(\kappa)e^{-i\mathbf{q}\cdot\mathbf{R}(\mathbf{l}')} - \mathbf{e}(\kappa')$, $\mathbf{e}(\kappa) - \mathbf{e}(\kappa')e^{i\mathbf{q}\cdot\mathbf{R}(\mathbf{l}')}$, and $\mathbf{e}^*(\kappa) - \mathbf{e}^*(\kappa')e^{-i\mathbf{q}\cdot\mathbf{R}(\mathbf{l}')}$, respectively. Finally, $\mathbf{S}_{0+}^{(1)}$, $\mathbf{S}_{0-}^{(1)}$, $\mathbf{S}_{+0}^{(1)}$, and $\mathbf{S}_{-0}^{(1)}$ are defined by similar expressions but with the matrix $\mathbf{H}$ replaced by the overlap matrix $\mathbf{S}$.

Similarly to the band energy, the repulsive energy E_{rep} is expanded in series of $u_\alpha(\mathbf{0}\kappa\mathbf{l}'\kappa')$ up to second order. The dynamical matrix is then derived from the expression

$$D_{\alpha\beta}(\kappa\kappa'|\mathbf{q}) = \frac{1}{M}\frac{\partial^2(E_{BS} + E_{rep})}{\partial e_\alpha(\kappa|\mathbf{q})\,\partial e_\beta(\kappa'|\mathbf{q})}, \tag{B5}$$

where M is the mass of the carbon atom. The phonon eigenvalues and eigenvectors can then be found as solutions to the phonon equations of motion.

APPENDIX C

We adopt the quantum-mechanical description of the Raman-scattering process in which the system of the electrons and the phonons of the system, and photons of the electromagnetic radiation, and their interactions are considered.[14] Restricting ourselves to Stokes processes, we retain only the terms of the Raman tensor, which give predominant contribution to the intensity close to resonance. These processes include (a) absorption of a photon (energy E_L, polarization vector $\boldsymbol{\epsilon}^L$) with excitation of the electronic subsystem from the ground state and creation of an electron-hole pair, (b) scattering of the electron (hole) by a phonon (frequency ω, polarization vector $\mathbf{e}$), and (c) annihilation of the electron-hole pair with emission of a photon (energy $E_S = E_L - \hbar\omega$, polarization vector $\boldsymbol{\epsilon}^S$) and return of the electronic subsystem to the ground state. The contribution of these processes to the Raman intensity is given by the expression[25]

$$I_0 = A\left|\sum \frac{p^S D p^{L*}}{(E_L - E - i\gamma_e)(E_S - E - i\gamma_e)}\right|^2. \tag{C1}$$

Here, $A = C(E_S^2/E_L^2)(n+1)$, C is a constant, n is the phonon Bose-Einstein distribution function, and γ_e is the excited-state width. $E \equiv E_{\mathbf{k}m'} - E_{\mathbf{k}m}$, where $\mathbf{k}m'$ and $\mathbf{k}m$ are states of the conduction and valence bands, respectively. $p^{L,S}$ is the matrix element of the component of the momentum in the direction of the polarization vector $\boldsymbol{\epsilon}^{L,S}$ and D is the electron-phonon coupling matrix element. The summation is performed over all wave vectors and over the conduction and valence bands.

Equation (C1) holds for infinite phonon lifetime. The phonons interact with other particles, e.g., phonons, electrons, etc., which decreases their lifetime and increases the phonon linewidth. Equation (C1) can be corrected for the case of a finite phonon linewidth by means of a Lorentzian broadening of the line[15]

$$I = \frac{1}{\pi}\frac{\Gamma}{(E_L - E_S - \hbar\omega - \Delta\omega)^2 + \Gamma^2}I_0. \tag{C2}$$

Here Γ is the total linewidth, equal to the sum of the broadening $\Delta\Gamma$ due to electron-phonon interactions and the contribution Γ_0 from other processes.

[1] K. S. Novoselov, A. K. Geim, S. V. Morozov, D. Jiang, Y. Zhang, S. V. Dubonos, I. V. Grigorieva, and A. A. Firsov, Science **306**, 666 (2004).
[2] C. Berger, Z. Song, X. Li, X. Wu, N. Brown, C. Naud, D. Mayou, T. Li, J. Hass, A. N. Marchenkov, E. H. Conrad, P. N. First, and W. A. de Heer, Science **312**, 1191 (2006).
[3] S. Pisana, M. Lazzeri, C. Casiraghi, K. S. Novoselov, A. K. Geim, A. C. Ferrari, and F. Mauri, Nature Mater. **6**, 198 (2007).
[4] J. Yan, Y. Zhang, Ph. Kim, and A. Pinczuk, Phys. Rev. Lett. **98**, 166802 (2007).
[5] X. Du, I. Skachko, A. Barker, and E. Y. Andrei, Nat. Nanotechnol. **3**, 491 (2008).
[6] A. Das, B. Chakraborty, S. Piscanec, S. Pisana, A. K. Sood, and A. C. Ferrari, Phys. Rev. B **79**, 155417 (2009).
[7] M. Lazzeri and F. Mauri, Phys. Rev. Lett. **97**, 266407 (2006).
[8] S. Piscanec, M. Lazzeri, F. Mauri, A. C. Ferrari, and J. Robertson, Phys. Rev. Lett. **93**, 185503 (2004).
[9] V. N. Popov and Ph. Lambin, Phys. Rev. B **74**, 075415 (2006).
[10] M. Mohr, J. Maultzsch, E. Dobardžić, S. Reich, I. Milosević, M. Damnjanović, A. Bosak, M. Krisch, and C. Thomsen, Phys. Rev. B **76**, 035439 (2007).
[11] V. N. Popov and Ph. Lambin, Phys. Rev. B **73**, 085407 (2006).
[12] V. N. Popov and L. Henrard, Phys. Rev. B **70**, 115407 (2004).
[13] D. Porezag, Th. Frauenheim, Th. Köhler, G. Seifert, and R. Kaschner, Phys. Rev. B **51**, 12947 (1995).
[14] R. M. Martin and L. Falicov, in *Topics of Applied Physics*, edited by M. Cardona (Springer, Berlin, 1975), Vol. 8.
[15] R. Loudon, Proc. R. Soc. London **275**, 218 (1963).
[16] S. Siebentritt, R. Pues, K.-H. Rieder, and A. M. Shikin, Phys. Rev. B **55**, 7927 (1997).
[17] J. Maultzsch, S. Reich, C. Thomsen, H. Requardt, and P. Ordejón, Phys. Rev. Lett. **92**, 075501 (2004).
[18] L. M. Malard, D. L. Mafra, S. K. Doorn, and M. A. Pimenta, Solid State Commun. **149**, 1136 (2009).
[19] A. Grüneis, J. Serrano, A. Bosak, M. Lazzeri, S. L. Molodtsov, L. Wirtz, C. Attaccalite, M. Krisch, A. Rubio, F. Mauri, and T. Pichler, Phys. Rev. B **80**, 085423 (2009).
[20] M. Lazzeri, C. Attaccalite, L. Wirtz, and F. Mauri, Phys. Rev. B **78**, 081406(R) (2008).
[21] H. Haken, *Quantum Field Theory of Solids: An Introduction* (North-Holland, Amsterdam, 1976).
[22] W. E. Pickett and P. B. Allen, Phys. Rev. B **16**, 3127 (1977).
[23] S. Piscanec, M. Lazzeri, J. Robertson, A. C. Ferrari, and F. Mauri, Phys. Rev. B **75**, 035427 (2007).
[24] C. M. Varma and W. Weber, Phys. Rev. B **19**, 6142 (1979).
[25] V. N. Popov, L. Henrard, and Ph. Lambin, Phys. Rev. B **72**, 035436 (2005).